Polish Journal of Medical Physics and Engineering
The Journal of Polish Society of Medical Physics
ISSN 1898-0309, doi: 10.2478/pjmpe-2024-0025

December 2024
Vol 30, Issue 4

Scientific Paper

Investigation of FLUKA Monte Carlo code to study the influence of degrader and initial proton energy in the Bragg peak position

Abdelkrim ZEGHARI[1,ABCDEF,*], Youssef BOUZEKRAOUI[2,CE], Karim BAHHOUS[1,C], Nourddine SLASSI[3,A], Rajaa CHERKAOUI EL MOURSLI[1,EF]

[1]*Physics, Faculty of Sciences, Mohammed V University, Rabat, Morocco*
[2]*Laboratory of Sciences and Health, High Institute of Health Sciences, Hassan First University, Settat, Morocco*
[3]*Medical Physics Department, HASSAN II Clinical, Fes, Morocco*
[*]*Corresponding author: Dr. Abdelkrim Zeghari; a.zeghari@um5s.net.ma*

(received 18 December 2023; revised 4 July 2024; accepted 13 August 2024)

Abstract

Introduction: In recent times, numerous leading global societies have endeavored to advance proton therapy technology with the aim of making it universally accessible. The goal is to offer proton therapy to all cancer patients who stand to benefit from it, thereby enhancing their overall quality of life. This shared objective unites radiation oncologists, medical physicists, radiotherapists, and hospital directors worldwide. The introduction of proton therapy systems, coupled with adjustments to the momentum analysis system, holds potential clinical benefits.

Material and Methods: The momentum analysis system typically modifies the energy of the clinical proton beam, influencing the shape and position of the Bragg peak. FLUKA, a Monte Carlo-based software, was employed to simulate various beam setups by directing the proton beam into a water phantom. The resulting Bragg peaks were analyzed and compared with those from different setup simulations.

Results: The findings indicate that the Bragg peak undergoes changes in a proton therapy system, both with and without a modulator, across all potential tumor depths. The results demonstrate that the position of the Bragg peak can vary from Z = 31.4 cm for deep tumors such as prostate to Z = 2.6 cm for spinal axis tumors, solely by adjusting the modulator depth from $\Delta Z_{\text{modulator}} = 5$ to $\Delta Z_{\text{modulator}} = 30$ cm for an energy level of 250 MeV, without altering the proton beam energies.

Conclusion: The investigation of these results plays a potential dosimetric consequence, especially for clinics interested in acquiring such a proton therapy system for treating and managing tumors at varying depths.

Keywords: FLUKA; proton therapy; dose distribution; Bragg-peak; modulator.

Introduction

Cancer is now considered one of the major diseases affecting people in developing countries. More than 55 percent of new cases are projected to rise by 2050, according to a Harvard study.[1] The International Agency for Research on Cancer (IARC) and the World Health Organization (WHO) suggest that cancer could increase by 50% to over 15 million new cases in 2023.[2]

Cancer can develop in almost every kind of tissue, whether on the skin or deep within the body. The treatment field needs to be adapted to treat every possible kind of cancer at any depth. A dose check is recommended before any treatment. The treatment plan defines all the beam parameters to be applied to completely destroy cancerous cells.

Therefore, the clinical application of such techniques requires a reliable estimate of the absorbed dose distributions to ensure a compromise between the need to sufficiently irradiate cancerous tissue and avoiding irradiation of neighboring healthy tissues. On that occasion, patient dosimetry becomes the stage where treatment planning can be evaluated, experimentally verified, and finally validated. Monte Carlo (MC) methods are increasingly utilized for clinical treatment planning in these situations. In 1927, the Norwegian physicist Widerøe R. developed the linear accelerator (linac).[3] Linacs are used for accelerating electrons in electron and photon therapy, but linacs for protons would be too long for clinical use. Fortunately, it is possible to gain higher kinetic energy by using circular accelerators. The cyclotron was invented in 1930 by Lawrence E. O.[4] It consists of two dipole magnets with a constant magnetic field B over a wide area. Charged particles are placed in the

Authors' contribution:
A – Research concept and design, B – Collection and/or assembly of data, C – Data analysis and interpretation, D – Writing the article, E – Critical revision of the article, F – Final approval of the article.

middle of the cyclotron, where they are accelerated in a cavity with electrical potential. In 1946, Robert R. Wilson proposed using fast protons in cancer therapy. He had worked on cyclotrons. He argued that the Bragg curve made an ideal depth dose curve for treating tumors and minimizing damage to healthy tissue. Robert R. Wilson hence marked the start of proton therapy and is today seen as the father of proton therapy.[5] During the next three decades, many research centers around the world started treating patients as part of their particle research, including Russia, Japan, and Switzerland. After 35 years of treating patients in research centers, the first full-scale clinical center was opened at Loma Linda Hospital in 1990.[6] It had its own designated synchrotron, made by physicists at Fermilab. Multiple treatment rooms for one single accelerator became the standard for most of the new centers, optimizing the cost per patient.

Recently, interest in radiation therapy with heavy ions such as protons has gained momentum. More than 200,000 patients were treated with protons in 110 centers around the world. The reason why proton therapy is preferred clinically is that higher doses can be given to the tumor compared to photon radiotherapy, providing better protection of healthy tissue.[7] Particle physics collaborations, for example, at CERN (l'Organisation Européenne pour la Recherche Nucléaire), have brought together thousands of scientists from every laboratory in the world to work on the largest and most complex experiments. Proton therapy could still be profitable due to the reduction of secondary tumors. While proton therapy could be very effective for children, e.g., with brain melanoma, the gain-to-cost ratio is still low for seniors, e.g., prostate cancer.[8,9] Cost-effectiveness would be one of the major focus areas of the community in the coming years. Proton therapy still has to prove that it is worth the money spent.

As a response to the high investment cost, most centers were based on multiple treatment rooms and one accelerator. Different companies today are delivering single-room centers. Two companies, IBA and Mevion, have installed the first centers and started treating patients. There are many approaches to cost reduction, like building smaller accelerators or smaller gantries.[10] The depth of the most distal edge of different tumor categories and their values have been read out and fitted together with the Norwegian overview of possible patients. The spinal axis is skin-close; the distal part of the planning treatment volume (PTV) is at most 6-7 cm from the surface of the back. However, for the prostate, the distal edge could be between 23 cm and 32 cm from the surface of the body. These 32 cm are the reason why the accelerators need to be able to accelerate the protons all the way to 250 MeV or more. An energy range of 230-250 MeV is the standard extraction energy of clinical cyclotrons today. It would still be possible to treat many patients by using smaller accelerators based on FLASH radiation therapy.[11] As an example, 50% of the patients could still be treated with a maximum range of 17 cm. Some companies chose an ingenious solution for their center; by mounting the cyclotron on the gantry, they were able to fit all the equipment into a single room. They also had the opportunity to treat from all angles and at all depths within the body. However, by implementing the cyclotron onto the gantry, there was no room for a momentum analyzer in the beam line. According to J. M. Schippers and A. J. Lomax,[12] the difference in energy spread would enlarge the distal dose falloff of the Spread Out Bragg Peak (SOBP), which again would yield an extra unnecessary dose to other organs nearby.[13,14] The extra organ dose is difficult to measure and changes from patient to patient. The distal dose falloff of a pristine Bragg peak is a generic and physical distance, independent of which supplier of the momentum analyzer-free system. The parameter was quantified for different treatment depths within the body by simulating a proton beam with an MC technique. By quantifying the distal dose falloff as a function of treatment depths, it is possible to compare the system with a momentum analyzer to the systems without a momentum analyzer. In this study, the Bragg curves of protons from 50 MeV to 250 MeV, in a step of ΔE = 20 MeV, were investigated inside a water phantom using the FLUKA MC simulation software. The Bragg curve dose of proton beams in the water phantom was calculated and compared with each other.

Materials and methods

Synchrotron/ESS Monte Carlo simulation

The FLUKA code CERN version V4-2.2 was employed in conjunction with graphical user interface software, Flair V.2.0--3, for dose calculations. A simple model, depicted in **Figure 1**, was constructed around a small water phantom. In each experiment, the proton beam was initiated at x = 0, y = 0, z = -150 cm and directed straight towards the water phantom. To enhance the experiment's realism, all parameters were sourced from other research papers (beam is initialized in z = -150 cm and the maximum energy spread at the PSI facility $\sigma_{E,0}$ = 1.2% of E_0).[15,16] The experiment involved comparing various main setups, each focusing on different parameters from different papers.[15,16] These setups were categorized into two groups: The Synchrotron/ESS setups and the Modulator setups, with the latter lacking the MAS (Momentum Analysis System).

The beam was initialized at Z = -150 cm with a variable energy E, a value extracted from the patent of the synchrotron at the Heidelberger Ionenstrahl Therapiezentrum (HIT), a modern particle therapy synchrotron.[15] A system with a full energy selection system (ESS) can adjust the energy spread σ_E by modifying the width of the momentum collimator.[16] A depth dose curve can be technically achieved by placing a colimator made of a high Z material in the beam between the source and the patient.[16,17]

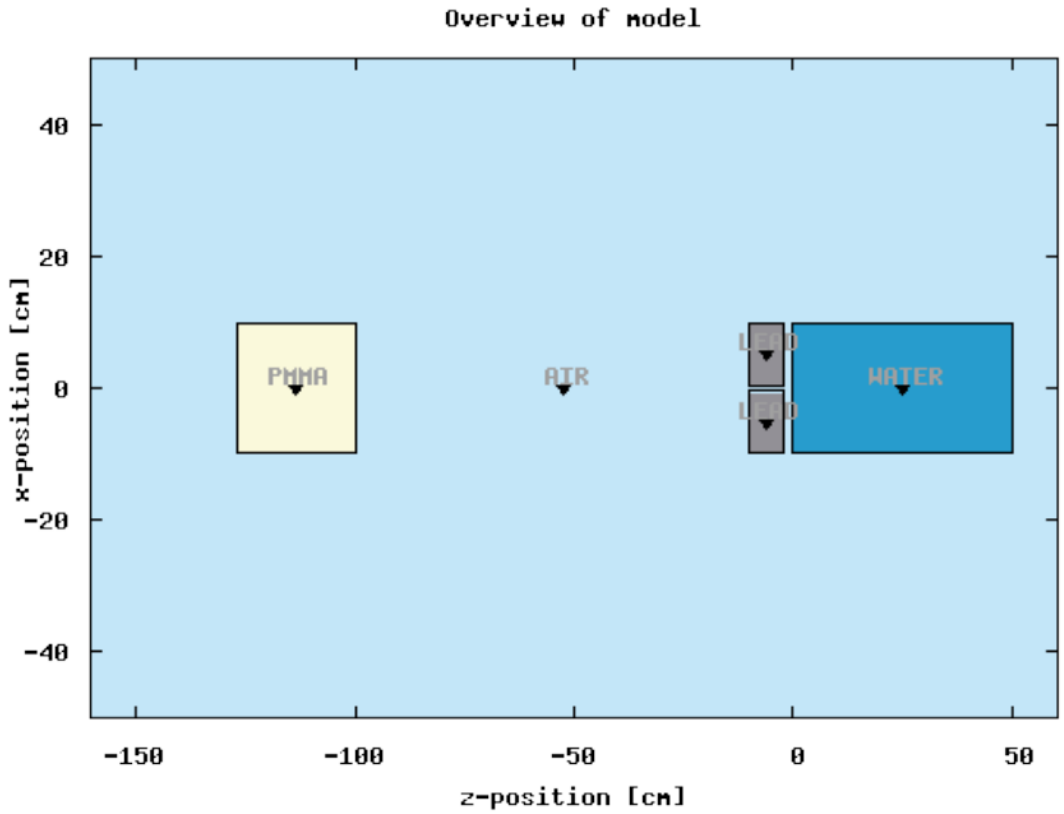

Figure 1. XZ view at y = 0 of the FLUKA model used in the Monte Carlo Simulation.

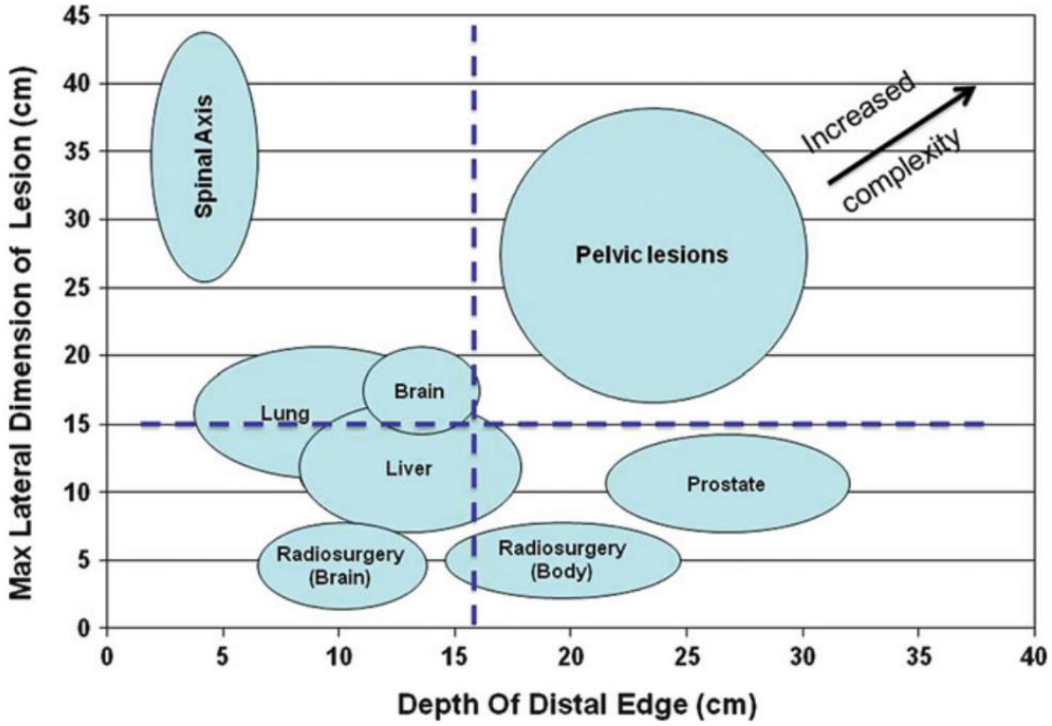

Figure 2. An illustration over the maximum lateral and distal limits of the treatment fields of different cancer categories.[21]

A 12 runs were simulated for the two synchrotron/ESS setups with different energies, at steps of ΔE = 20 MeV from E = 50 MeV to E = 270 MeV without the modulator. Then, 6 runs were simulated for different modulator materials. After that, we simulated a total of 17 runs for modulator thickness, in steps of $\Delta Z_{modulator}$ = 5 cm: from $\Delta Z_{modulator}$ = 0 cm to $\Delta Z_{modulator}$ = 25 cm for energies 230 MeV, then from $\Delta Z_{modulator}$ = 5 cm to $\Delta Z_{modulator}$ = 30 cm for energies 250 MeV, and finally from ΔZ modulator = 10 cm to $\Delta Z_{modulator}$ = 30 cm for energies 270 MeV. Also, we ran five simulations for different collimator materials.

Each run tracked 1×10^6 initial protons, providing an "acceptable" error for most simulations (typically 1-2%). The dose ($Gy \times cm^2 / 10^6$ protons) was measured in the water phantom along the axis using a cylindrical detector. The results were then plotted with the Gnuplot program to illustrate the different depth-dose curves for the full Bragg peaks in all setups. Additionally, a lateral map of the x-axis was generated to depict the lateral spread. All simulations were conducted on a desktop with an Intel Core i7 CPU, 16 GHz RAM, running on the Ubuntu 20.04. system, utilizing the FLUKA/FLAIR code.

Modulator and momentum analysis system

In recent active scanning nozzles have no components in the trajectory of the beam; a simple synchrotron/ESS setup is easy to model. But a compact proton therapy system would be a bit more complex, since all beam components need to be placed in the nozzle, between the accelerator and the patient. The Mevion S250 was the only kind of compact therapy system without a momentum analysis system (MAS).[18] Since we are interested in looking at the Bragg-Peak dependency, we could further simplify the model to only include the modulator. Cyclotrons are only able to extract their beam at the maximum treatment energy, so the beam has to be modulated to achieve lower energies. The modulator is most certainly made of a material with low Z, which relatively stops the beam more than it scatters, compared to high Z material. In our model, the modulator is then set to Poly Methyl Meth Acrylate (PMMA), a typical material in a modulator. In the synchrotron/ESS setups, the initial energy E is varied to change the range, while in the modulator setup, the thickness of the modulator is varied. The beam can be adjusted so that the Bragg peak is placed at the tumor site.

The proton energy is changed by passing the beam through a modulator and many Bragg peaks occur at various depths. The modulator (degrader) is able to change the energy by adjusting the thickness of the material which the beam has to pass through the different tumor depth categories as indicated in **Figure 2**.

The energy adjustment should be done as fast as possible to get rid of interpolation effects, one of the greatest issues in modern proton therapy.[16] To mimic a realistic beam of a system without a MAS, the initial beam parameters are taken from research papers about the Mevion system. The beam is initialized with an energy E = 250 MeV in the positive z-direction at Z = -150 cm.[18] Parodi and Enghardt, in a research paper, take the energy spread from the synchrocyclotron as σ_E = 0.42 MeV.[19] The protons also scatter a lot in the modulator, which will widen the focus of the beam at the phantom water entrance. This could be done by a small passive collimator of lead with a circular hole. In a paper about the passive scattering system in Mevion, a passive high Z collimator is placed 2 cm in front of the water phantom.[17] The collimator thickness is set to a constant of 8 cm to ensure there will be no radiation behind, even though such a metal is far to heavy for clinical use. In the conference proceeding by Bloch et al., the σ_E value from the accelerator was chosen to be 1.4 MeV, based on fitting σ_E to measurements on the first Mevion S250 in clinical use.[18]

Bragg curve and range straggling

The Bragg curve, which is the relative depth dose curve, derives its characteristic shape from three main interactions occurring between the accelerated protons and matter. The shape of the ionization curve is strongly dependent on the energy of the protons. Range straggling, a phenomenon where the protons travel into matter before coming to a halt. The mean range R can be calculated using the "continuous slowing down approximation", by integrating over the stopping power for energy from E to 0:[20]

$$R(E) = \alpha \cdot E^p \qquad \text{Eq. 1}$$

All particle interactions (stopping, scattering, and nuclear interactions) are randomized processes. So, the particles in a beam will not have the same number of collisions. So, every proton would not have the same range in the material, even for mono-energetic protons in a homogeneous material.[21]

The International Commission on Radiation Units & Measurements (ICRU) has experimentally given $\alpha = 2.2 \times 10^{-3}$ cm·MeV and p = 1.77 for protons passing through water.[22]

Results and Discussions

The presented FLUKA-based tool is capable of calculating the depth dose ($Gy \times cm^2 / 10^6$ protons) curve for all kinds of geometrical configurations and incident beams.

Figure 3 shows a comparison of different FLUKA-calculated depth doses of Bragg peaks on a water phantom for some energy values ranging from 50 MeV to 250 MeV beams. It is evident that the contribution of proton particles due to principal interactions influences the distribution of the position of Bragg peaks' dose. It is clear that the increase in energy towards the water phantom raises the position of Bragg peaks. These investigations have been conducted to understand the contributions of biological assessments.[13,14,16,23-25] **Table 1** shows a different FLUKA-calculated depth position of Bragg peaks on a water phantom for energy values ranging from 50 MeV to 250 MeV beams. **Figure 4** exposes the absorbed dose distribution (x,z) profile along the z-axis 250 MeV **(a)**, 230 MeV **(b)**, 210 MeV **(c)**, 90 MeV **(d)**, 70 MeV **(e)**, and 50 MeV **(f)**.

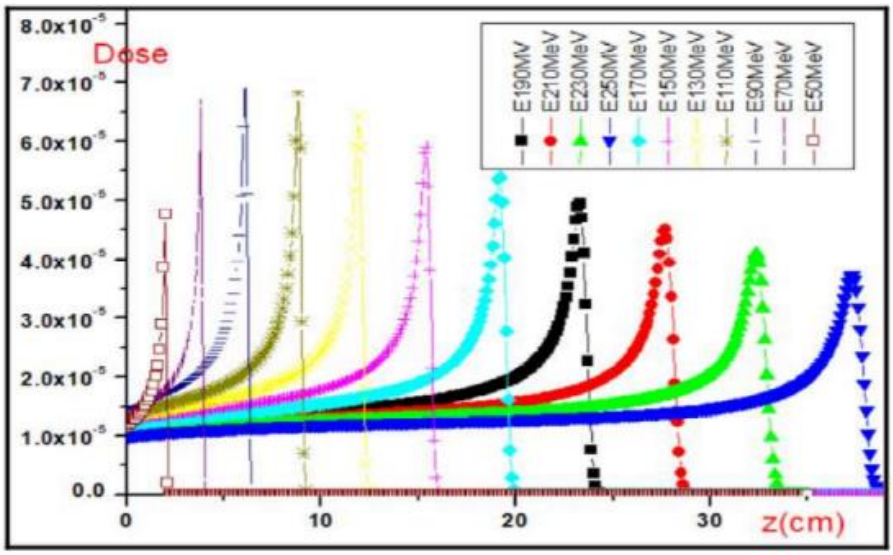

Figure 3. Absorbed dose as a function of depth z in a water phantom from a proton Bragg peak produced by a broad proton beams with an initial energies from 50 MeV to 250 MeV.

Table 1. MC calculated ranges for 50, 150 and 230 MeV primary proton energies in the water phantom.

Energy (MeV)	50	70	90	110	130	150	170	190	210	230	250
Bragg Peak (cm) FLUKA	2	3.8	6.1	8.8	11.9	15.4	19.2	23.3	27.7	32.3	37.3
Brag Peak (cm) [22] Gate/Geant4	2.22	-	-	-	-	15.73	-	-	-	32.86	-
Brag Peak (cm) [22] MCNP6	2.22					15.69				32.74	
Marius[23]	-	-	-	-	-	15.5	-	-	-	-	-

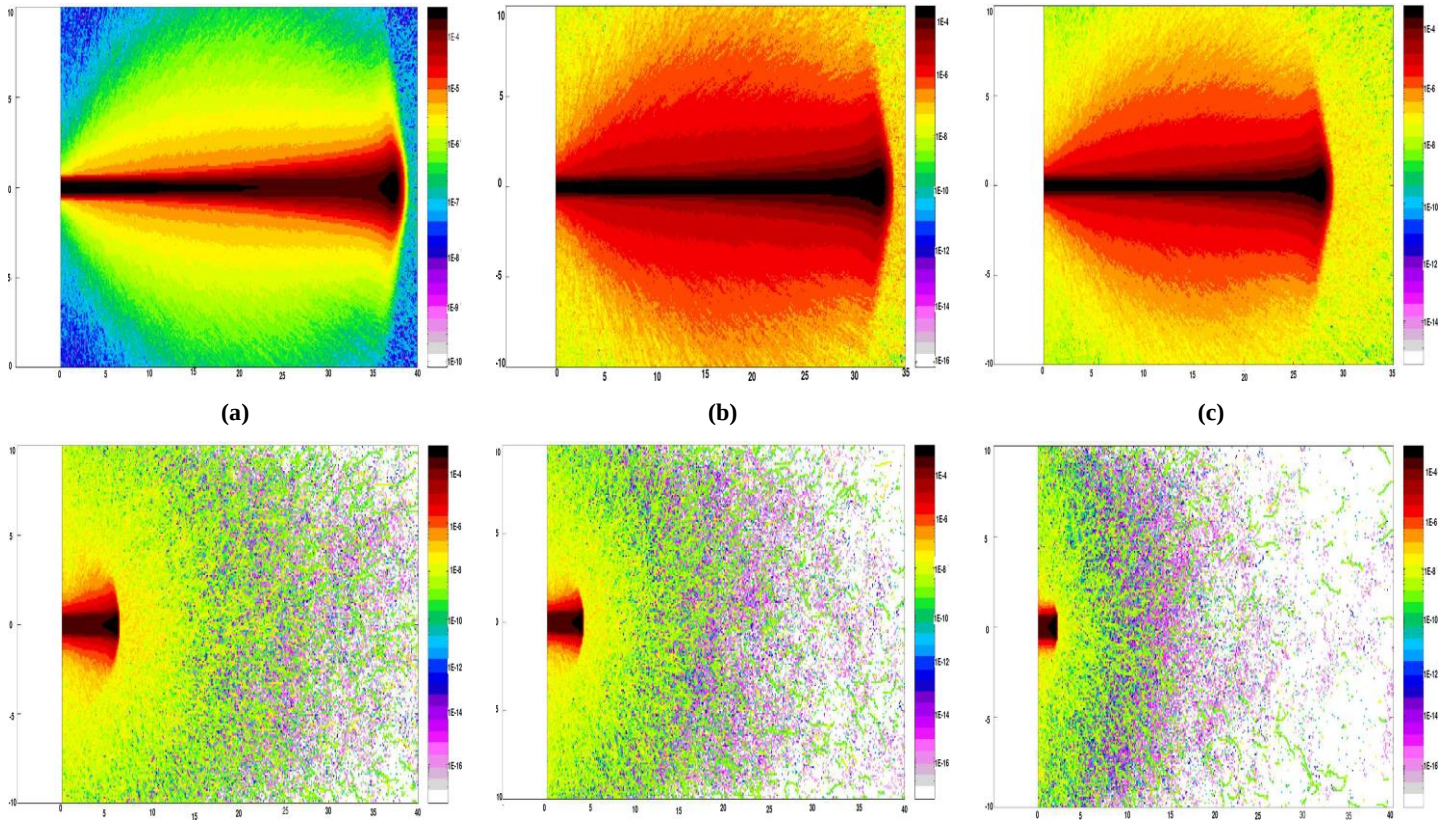

(a) **(b)** **(c)**

(d) **(e)** **(f)**

Figure 4. Energy deposition (x,z) profile of energies of 250, 230, 210, 90, 70 and 50 MeV protons inside the water phantom simulated using FLUKA-USRBIN.

Figure 5 illustrates the variation of depth dose distributions of 230 MeV proton beams inside a water phantom with a modulator thickness altered from $\Delta Z_{modul} = 0$ to $\Delta Z_{modul} = 25$ cm. **Figure 6** presents the depth dose distributions of 250 MeV proton beams inside a water phantom with a modulator thickness changed from $\Delta Z_{modul} = 5$ cm to $\Delta Z_{modul} = 30$ cm. **Figure 7** illustrates the variation of depth dose distributions of 270 MeV proton beams inside a water phantom with a modulator thickness varied from $\Delta Z_{modul} = 10$ to $\Delta Z_{modul} = 30$ cm. **Figure 8** presents the depth dose distributions of 250 MeV proton beams inside a water phantom when we changed the modulator materials to include PMMA, Polyethylene, Polystyrene, and Plastic Scintillator. Figure 9 illustrates the depth dose distributions of 250 MeV proton beams inside a water phantom with a collimator made of different materials. As a starting point for discussion, this section examines the influence of the physical and radiobiological properties of proton beams, which offer superior dose distribution inside the localized target compared to photon radiotherapy, by minimizing the dose to normal tissues proximal and distal to the tumor.

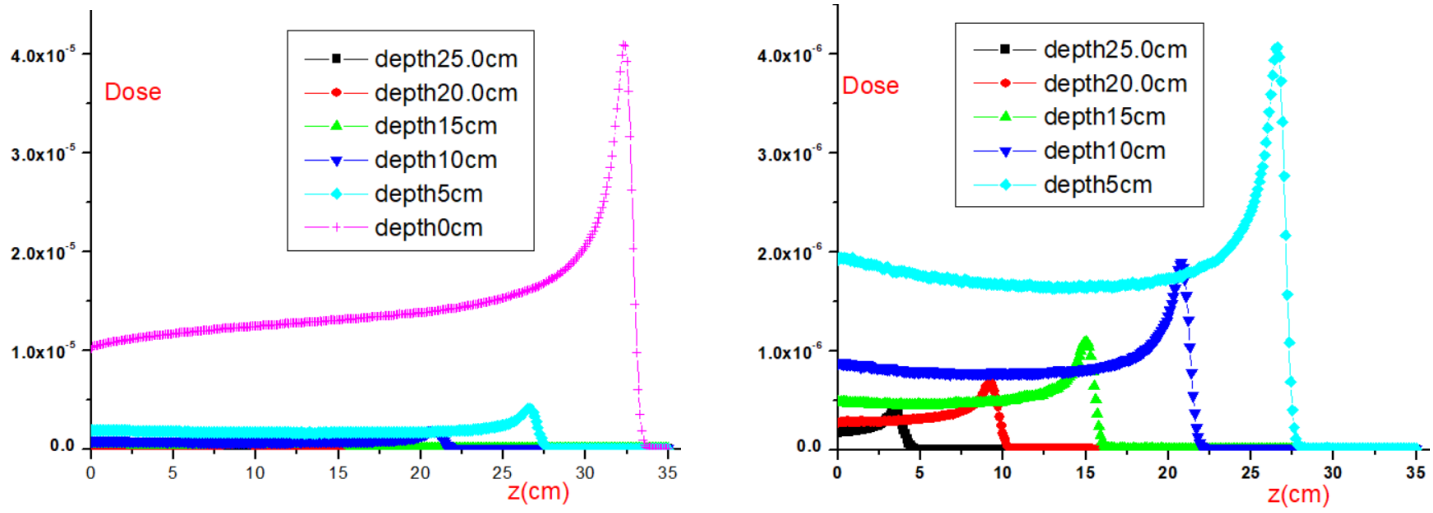

(a) (b)

Figure 5. Depth dose distributions of 230 MeV proton beams inside a water phantom with depth modulator from $\Delta Z_{modul} = 0$ to $\Delta Z_{modul} = 25$ cm.

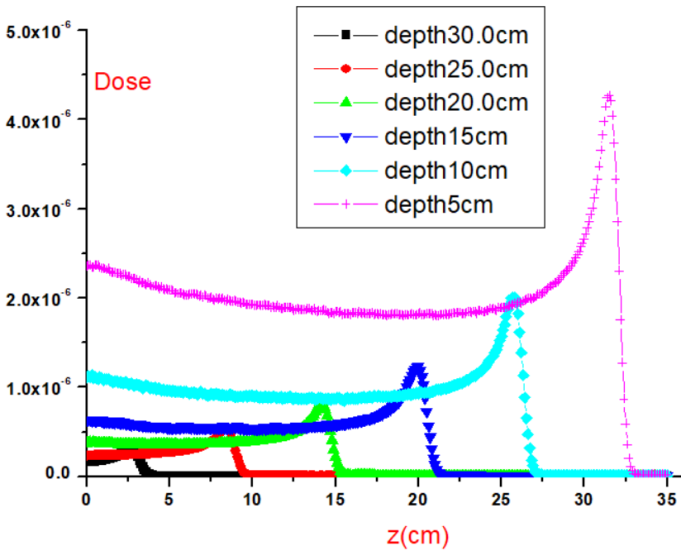

Figure 6. Depth dose distributions for 250 MeV proton beams inside a water phantom with depth modulator from $\Delta Z_{modul} = 5$ to $\Delta Z_{modul} = 30$ cm.

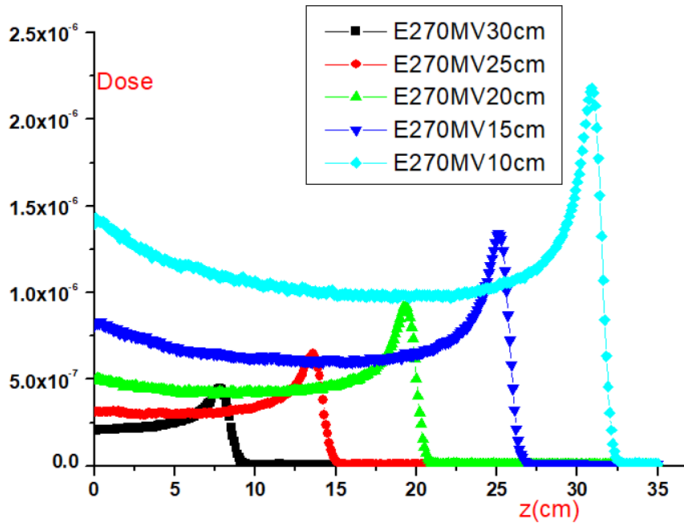

Figure 7. Depth dose distributions of 270 MeV proton beams inside a water phantom with depth modulator from ΔZ_{modul} =10 to ΔZ_{modul} = 30 cm.

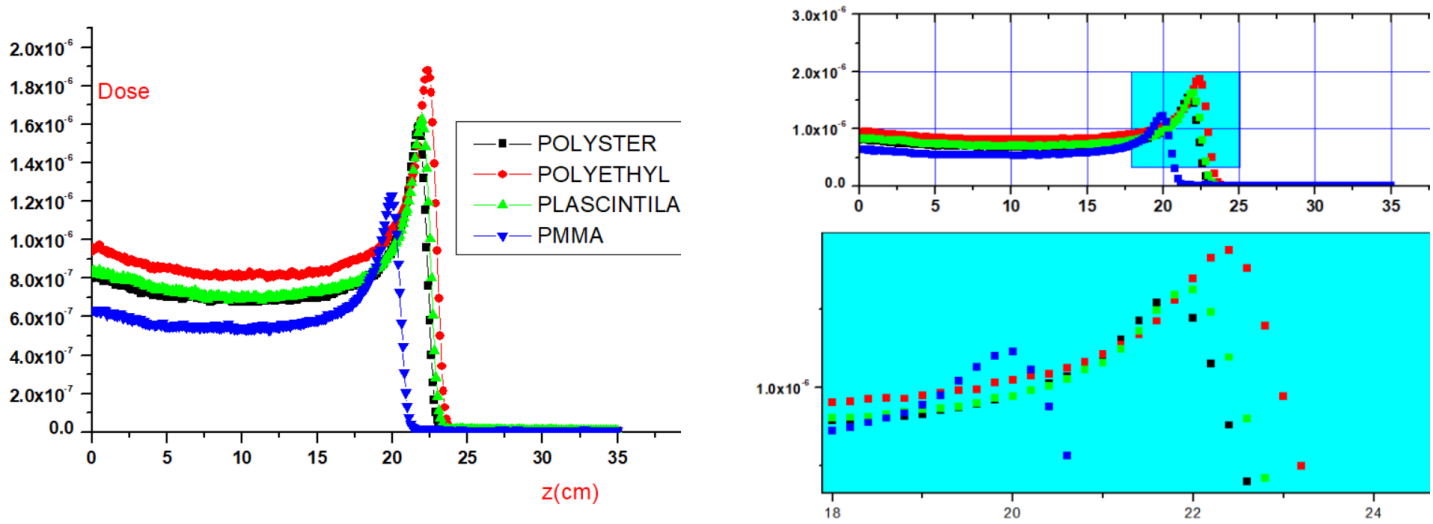

Figure 8. Depth dose distributions of 250 MeV proton beams inside a water phantom for different modulator materials (PMMA, Polyethylene, Polystyrene, Plastic Scintillator).

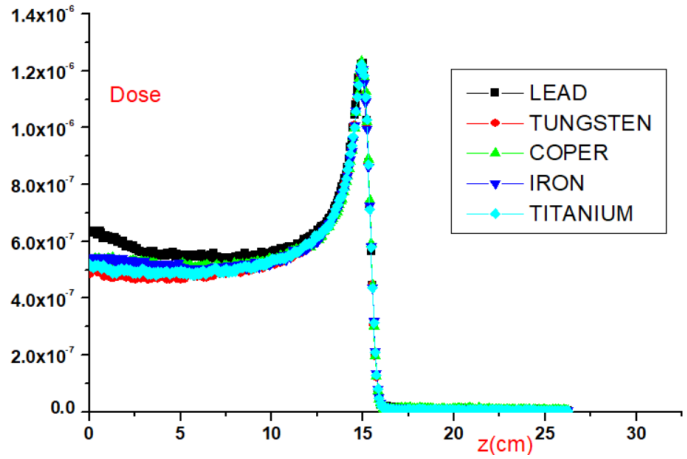

(a)

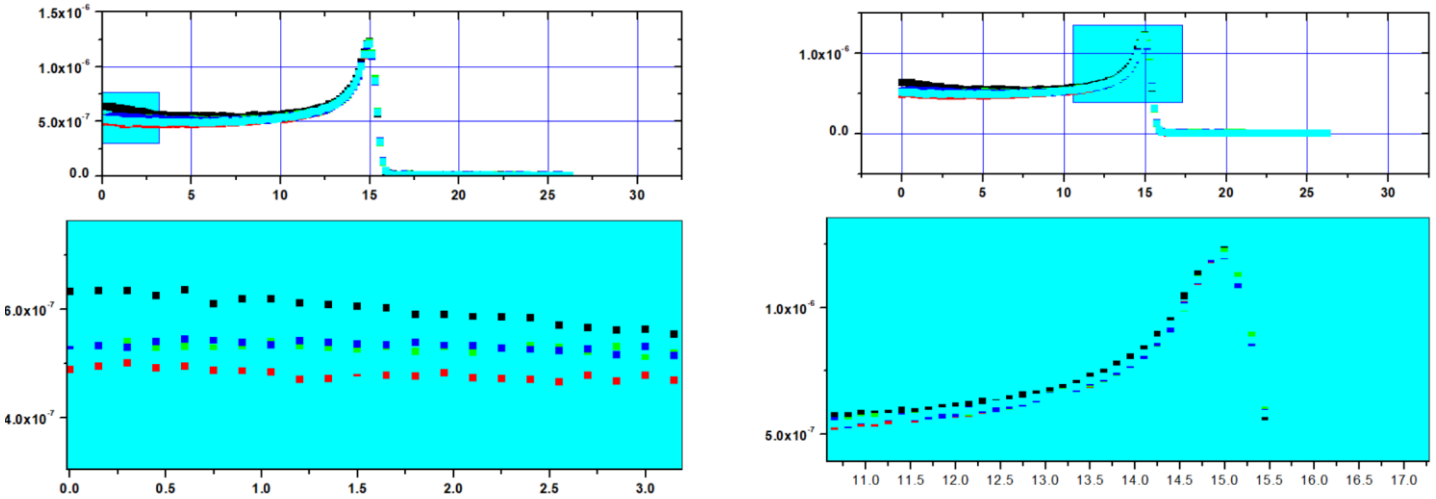

(b) **(c)**

Figure 9. Depth dose distributions of 250 MeV proton beams inside a water phantom with varied collimator materials.

The study investigates the variation of modulator thickness and materials on the position of the Bragg peak.[26-27] **Figure 3** depicts proton beams with different initial energies without a modulator, altering the Bragg peak position from Z = 37.3 cm for 250 MeV to Z = 1.8 cm for energy 50 MeV, creating a continuous spectrum of absorbed dose in diverse tumor regions. **Figure 4** displays the energy deposition (x,z) profile of protons with energies ranging from 50 MeV to 250 MeV inside a water phantom simulated using FLUKA-USRBIN. **Figure 5** illustrates various thicknesses of PMMA from $\Delta Z_{\text{modul, PMMA}} = 0$ to $\Delta Z_{\text{modul, PMMA}} = 25$ cm for 230 MeV, creating a continuous spectrum of absorbed dose in the tumor region based on the Bragg peak position. The effect of modulator PMMA material thickness was crucial, registering a reduction of the Bragg peak position from Z = 32.3 for $\Delta Z_{\text{modul, PMMA}} = 0$ cm to Z = 3.5 cm for $\Delta Z_{\text{modul, PMMA}} = 25$ cm.

Figure 6 shows the influence of different PMMA thicknesses from $\Delta Z_{\text{modul,PMMA}} = 5$ to $\Delta Z_{\text{modul,PMMA}} = 30$ cm for 250 MeV, registering a reduction of the Bragg peak position from Z = 31.4 for $\Delta Z_{\text{modul, PMMA}} = 5$ cm to Z = 2.6 cm for $\Delta Z_{\text{modul, PMMA}} = 30$ cm. **Figure 7** illustrates the influence of different PMMA thicknesses from Z=10 to Z=30 cm for 270 MeV, registering a reduction of the Bragg peak position from Z = 30.9 for $\Delta Z_{\text{modul,,PMMAA}} = 10$ cm to Z = 2.6 cm for $\Delta Z_{\text{modul, PMMA}} = 30$ cm. Figure 8 shows the variation of the Bragg peak position with different modulator materials. The effect of modulator material was significant, registering a slight increase in the Bragg peak position when replacing PMMA with Polyethylene material from Z = 20 to Z = 22.3 cm.[17,25,26]

Figure 9 illustrates the variation of the Bragg peak position with different collimator materials. The effect of the colimator material was not significant on the Bragg peak position when substituting Lead material, but a small decrease in entrance dose by a factor of 1.3 was observed when replacing the Lead collimator with a Tungsten collimator. Simulation results show that when the proton beam has an energy of 230 MeV without a degrader and 250 MeV with $\Delta Z_{\text{modul, PMMA}} = 5$ cm and 270 MeV with $\Delta Z_{\text{modul, PMMA}} = 10$ cm, the Bragg peak forms at the end of the tumor region. Our research uses low Z materials, such as PMMA, to change the range of protons, and high Z materials in the collimator, such as lead, to induce lateral scattering. Simulation of the 250 MeV proton beam with different modulator thicknesses shows the creation of several Bragg peaks in the tumor region. Consequently, an increase in modulator thickness demonstrates that the created Bragg peaks cover the entire tumor volume.

Conclusion

In this study, the performance of the FLUKA particle therapy tool in the clinical environment was presented. Our MC model was constructed for a range of 50-250 MeV proton beams incident as Magnetic Analysis System (MAS) accelerators on a cubic water phantom. This paper investigates different depths and materials for the modulator system and various materials for the collimator on Bragg curves calculated with the FLUKA/FLAIR MC code. This work shows the increase in energy towards the water phantom raises the position of Bragg peaks. The principal results of this paper establish that when different depths and materials for the modulator were investigated in FLUKA MC, the Bragg curve's position registered a significant variation. Also, we can say that the dose distributions results are sensitive to the variation of different materials for the collimator.

This study compared proton beams on the water phantom using Bragg curves and the lateral straggle energy doses. The findings revealed that the proton beam reached the same range using a modulator for high-energy 250 MeV compared to an average of 4 times less energy. In other words, the proton beam is more advantageous because it has a shorter range with high energy without changing the energy by only placing a modulator system.

In conclusion, the FLUKA MC code is used during the simulation workflow to improve the usability of the particle therapy tool for medical applications. So, this paper improves the usability of the proton therapy tool and extends the range of applications for the clinical and research environment.

References

1. Frenk J. Cancer is on the rise in developing countries. Harvard T.H. Chan School of Public Health. Available at: https://www.hsph.harvard.edu/news/magazine/shadow-epidemic/
2. Cancer. World Health Organization. Available at: https://www.who.int/news-room/fact-sheets/detail/cancer
3. Wiik BH. Rolf Wideröe and the Development of Particle Accelerators. Acta Oncologica. 1998;37(6):615-625. https://doi.org/10.1080/028418698430322
4. Lawrence EO, Edlefsen NE. On the production of high speed protons. Science. 1930;72:376
5. Wilson RR. Radiological Use of Fast Protons. Radiology. 1946;47(5):487-491. https://doi.org/10.1148/47.5.487
6. Slater JM, Archambeau JO, Miller DW, Notarus MI, Preston W, Slater JD. The proton treatment center at Loma Linda University Medical Center: Rationale for and description of its development. International Journal of Radiation Oncology*Biology*Physics. 1992;22(2):383-389. https://doi.org/10.1016/0360-3016(92)90058-p

7. Dowdell SJ. Pencil beam scanning proton therapy: the significance of secondary particles. Doctor of Philosophy thesis. University of Wollongong. Centre for Radiation Physics, University of Wollongong, 2011. https://ro.uow.edu.au/theses/3275
8. Konski A, Speier W, Hanlon A, Beck JR, Pollack A. Is Proton Beam Therapy Cost Effective in the Treatment of Adenocarcinoma of the Prostate? JCO. 2007;25(24):3603-3608. https://doi.org/10.1200/jco.2006.09.0811
9. Björk-Eriksson T, Glimelius B. The potential of proton beam therapy in paediatric cancer. Acta Oncologica. 2005;44(8):871-875. https://doi.org/10.1080/02841860500355959
10. Schippers JM, Lomax A, Garonna A, Parodi K. Can Technological Improvements Reduce the Cost of Proton Radiation Therapy? Seminars in Radiation Oncology. 2018;28(2):150-159. https://doi.org/10.1016/j.semradonc.2017.11.007
11. Schulte R, Johnstone C, Boucher S, et al. Transformative Technology for FLASH Radiation Therapy. Applied Sciences. 2023;13(8):5021. https://doi.org/10.3390/app13085021
12. Schippers JM, Lomax AJ. Emerging technologies in proton therapy. Acta Oncologica. 2011;50(6):838-850. https://doi.org/10.3109/0284186x.2011.582513
13. Bloch C, Hill PM, Chen KL, Saito A, Klein EE. Startup of the Kling Center for Proton Therapy. AIP Conference Proceedings. Published online 2013:314-318. https://doi.org/10.1063/1.4802340
14. Michaelidesová A, Vachelová J, Puchalska M, et al. Relative biological effectiveness in a proton spread-out Bragg peak formed by pencil beam scanning mode. Australas Phys Eng Sci Med. 2017;40(2):359-368. https://doi.org/10.1007/s13246-017-0540-8
15. Combs SE, Ellerbrock M, Haberer T, et al. Heidelberg Ion Therapy Center (HIT): Initial clinical experience in the first 80 patients. Acta Oncologica. 2010;49(7):1132-1140. https://doi.org/10.3109/0284186x.2010.498432
16. Kostromin SA, Syresin EM. Trends in accelerator technology for hadron therapy. Phys Part Nuclei Lett. 2013;10(7):833-853. https://doi.org/10.1134/s1547477114010154
17. Titt U, Zheng Y, Vassiliev ON, Newhauser WD. Monte Carlo investigation of collimator scatter of proton-therapy beams produced using the passive scattering method. Phys Med Biol. 2007;53(2):487-504. https://doi.org/10.1088/0031-9155/53/2/014
18. Chen KL, Bloch CD, Hill PM, Klein EE. Evaluation of neutron dose equivalent from the Mevion S250 proton accelerator: measurements and calculations. Phys Med Biol. 2013;58(24):8709-8723. https://doi.org/10.1088/0031-9155/58/24/8709
19. Parodi K, Enghardt W. Potential application of PET in quality assurance of proton therapy. Phys Med Biol. 2000;45(11):N151-N156. https://doi.org/10.1088/0031-9155/45/11/403
20. Bragg WH, Kleeman R. XXXIX. On the α particles of radium, and their loss of range in passing through various atoms and molecules. The London, Edinburgh, and Dublin Philosophical Magazine and Journal of Science. 1905;10(57):318-340. https://doi.org/10.1080/14786440509463378
21. Cameron J, Schreuder N. Smaller – Lighter – Cheaper: New Technological Concepts in Proton Therapy. Biological and Medical Physics, Biomedical Engineering. Published online September 6, 2011:673-685. https://doi.org/10.1007/978-3-642-21414-1_40
22. ICRU Report 49, International Commission on Radiation Units and Measurements: Stopping Powers and Ranges for Protons and Alpha Particles (Bethesda, Maryland, USA). 1993.
23. Pavlovič M, Hammerle A. Ranges of protons in biological targets. Journal of Electrical Engineering. 2017;68(4):306-311. https://doi.org/10.1515/jee-2017-0043
24. Linz U, ed. Ion Beam Therapy. Springer Berlin Heidelberg; 2012. https://doi.org/10.1007/978-3-642-21414-1
25. Sølie JR, Pettersen HES, Meric I, Odland OH, Helstrup H, Röhrich D. A comparison of proton ranges in complex media using GATE/Geant4, MCNP6 and FLUKA. Published online 2017. https://doi.org/10.48550/ARXIV.1708.00668
26. Ekinci F, Bostanci E, Dagli Ö, Guzel MS. Analysis of Bragg curve parameters and lateral straggle for proton and carbon beams. CommunFacSciUnivAnkSeries A2-A3: PhysSci and Eng. 2021;63(1):32-41. https://doi.org/10.33769/aupse.864475
27. Hu M, Jiang L, Cui X, Zhang J, Yu J. Proton beam therapy for cancer in the era of precision medicine. J Hematol Oncol. 2018;11(1). https://doi.org/10.1186/s13045-018-0683-4